



INTERNATIONAL CONFERENCE ON WATER RESOURCES, COASTAL AND OCEAN
ENGINEERING (ICWRCOE 2015)

CFD Simulations of Wave Propagation and Shoaling over a Submerged Bar

Arun Kamath^{a*}, Hans Bihs^a, Mayilvahanan Alagan Chella^a, Øivind A. Arntsen^a

^aDepartment of Civil and Transport Engineering, NTNU, Trondheim 7491, Norway

Abstract

The wave propagation over a submerged bar is simulated using the open source CFD model REEF3D and the numerical results are compared to the experimental data. The transformation of the wave resulting in higher harmonics in the wave train is observed as the wave propagates over the crest of the bar. The difference between the wave transformation processes for two different incident wave heights is studied. The higher incident wave height shows more shoaling than the lower incident wave height. The numerical results show a good agreement with the experimental data.

© 2015 The Authors. Published by Elsevier B.V. This is an open access article under the CC BY-NC-ND license

(<http://creativecommons.org/licenses/by-nc-nd/4.0/>).

Peer-review under responsibility of organizing committee of ICWRCOE 2015

Keywords: Numerical wave tank ; wave generation and absorption; CFD

1. Introduction

Waves propagating from deep water to coastal shallow water are affected by the bottom topography, resulting in wave refraction, shoaling and breaking. The study of these processes is important in coastal engineering due to their significant impact on wave forces, wave run up and sediment transport, which influence the design of coastal structures. Wave transformation and breaking in shallow waters is investigated through the study of wave propagation over submerged structures and varying bottom topography to obtain a better understanding of the physical processes involved. Several studies have dealt with wave propagation and transformation over a submerged object through experimental investigations [Beji and Battjes (1993), Chang *et al.* (2001), Blenkinsopp and Chaplin (2008)], using Boussinesq-type equations [(Brocchini *et al.* 1992), Beji and Battjes (1994)] and shallow water equations (Kobayashi *et al.* 1987).

* Corresponding author.

E-mail address: arun.kamath@ntnu.no

The numerical models based on Boussinesq and shallow water equations can be only used to calculate the wave deformation due to shoaling but cannot be applied to directly model wave breaking (Christensen 1998). Wave breaking involves complex hydrodynamics involving the interaction of air and water in the evolution of the free surface, effects of fluid viscosity and turbulence. These effects cannot be represented using models based on potential theory, Boussinesq equations or single-phase numerical models. The application of Computational Fluid Dynamics (CFD) models solving the flow problem for both air and water phases can provide a detailed description of the deformation of the free surface during shoaling and breaking of waves. Jacobsen *et al.* (2011) presented the application of CFD to model spilling breaking waves using a wave toolbox in OpenFOAM and obtained a good agreement with the experimental results. Alagan Chella *et al.* (2015) validated the open source CFD model REEF3D for spilling breakers over a slope using experimental data from Ting and Kirby (1996) and investigated the influence of water depth, wave steepness and bottom slope on the geometric properties and characteristics of spilling breakers. Thus, the use of CFD modeling to investigate wave transformation and breaking in shallow water is a highly relevant application in the field of coastal engineering.

The objective of this study is to numerically investigate the wave transformation during over a submerged bar based on the experiments carried out by Beji and Battjes (1993). The experiments investigated the transformation of a periodic regular wave over a bar, involving transfer of wave energy among its higher harmonics. The numerical results are compared to the experimental data and the transformation of the free surface for different incident wave heights is examined to obtain more insight into the wave transformation process.

Nomenclature

u_i, u_j, u_k	velocity components along the x -, y - and z -axis
ρ	density
p	pressure
ν	kinematic viscosity
ν_t	eddy viscosity
g	acceleration due to gravity
ϕ	level set function
Γ	relaxation function
η	free surface elevation
u	horizontal water particle velocity
w	vertical water particle velocity
L	incident wavelength
k	incident wave number
H	incident wave height
T	incident wave period
dx	grid size
d	water depth

2. Numerical Model: REEF3D

The incompressible Reynolds Averaged Navier Stokes (RANS) equations are used to solve the fluid flow problem:

$$\frac{\partial u_i}{\partial x_i} = 0 \quad (1)$$

$$\frac{\partial u_i}{\partial t} + u_j \frac{\partial u_i}{\partial x_j} = -\frac{1}{\rho} \frac{\partial p}{\partial x_i} + \frac{\partial}{\partial x_j} \left[(v + v_t) \left(\frac{\partial u_i}{\partial x_j} + \frac{\partial u_j}{\partial x_i} \right) \right] + g_i \quad (2)$$

where u_i is the time averaged velocity, ρ is the density of water, p is the pressure, ν is the kinematic viscosity, ν_t is the eddy viscosity, t is time and g is the acceleration due to gravity. The pressure is treated using Chorin's projection method (Chorin 1968) and the resulting Poisson pressure equation is solved using a preconditioned BiCGStab solver (van der Vorst 1992). Turbulence modeling is carried out using the two-equation $k-\omega$ model proposed by Wilcox (1994). Eddy viscosity, ν_t , is bounded to avoid unphysical overproduction of turbulence in strained flow by using a stress limiter in the definition of eddy viscosity (Bradshaw *et al.* 1967) as shown by Durbin (2009). The large difference in density of air and water in a two-phase model leads to an overproduction of turbulence at the interface due to the large strain. Free surface turbulence damping as shown by Naot and Rodi (1982) is carried out to avoid the unphysical over production of turbulence at the interface. The damping is carried out only around the interface using the Dirac delta function.

The fifth-order conservative finite difference Weighted Essentially Non-Oscillatory (WENO) scheme proposed by Jiang and Shu (1996) is used for the discretization of convective terms for the velocity u_i , the level set function ϕ , turbulent kinetic energy k and the specific turbulent dissipation rate ω . A TVD third-order Runge-Kutta explicit time scheme developed by Shu and Osher (1988) is employed for time discretization in the model. This is a three-step scheme and involves the calculation of the spatial derivatives three times per time step. This scheme is used for the time advancement of the level set function and the re-initialization equation. An adaptive time stepping approach is used to maintain the time step in accordance with the Courant-Frederich-Lewy (CFL) criterion for numerical stability. The computational efficiency of the program is increased by parallelizing the code using MPI (Message Passing Interface). Here the domain is decomposed into smaller pieces and each assigned to a processor. So the program runs separately on each processor and the values between the processes are communicated using the MPI library.

The free surface is obtained using the level set method where the zero level set of a signed distance function is used to represent the interface between air and water (Osher and Sethian 1988). Moving away from the interface, the level set function gives the closest distance of the point from the interface. The sign of the function represents the two fluids across the interface as shown in Eq. (3).

$$\phi(\bar{x}, t) \begin{cases} > 0 & \text{if } \bar{x} \text{ is in phase 1} \\ = 0 & \text{if } \bar{x} \text{ is at the interface} \\ < 0 & \text{if } \bar{x} \text{ is in phase 2} \end{cases} \quad (3)$$

The velocity field in the simulation moves the level set function using the convection equation shown in Eq. (4):

$$\frac{\partial \phi}{\partial t} + u_j \frac{\partial \phi}{\partial x_j} = 0 \quad (4)$$

The signed distance property of the function is lost on convection and it is re-initialized after every iteration using a partial differential equation (PDE) based re-initialization procedure presented by Peng *et al.* (1999), to retain its signed distance property after convection.

A uniform Cartesian grid is used in the numerical model for spatial discretization. The Immersed Boundary Method (IBM) is used to incorporate the boundary conditions for complex geometries. In the current study, a local directional ghost cell IBM presented by Berthelsen and Faltinsen (2008) is implemented using object oriented programming techniques, where the ghost cell values can be updated from multiple directions Bihs (2011). The ghost cells store multiple values and return a particular value when called from the respective direction.

The relaxation method (Mayer *et al.* 1998) is used for wave generation and absorption in the numerical wave tank. This method uses a wave generation zone and a wave absorption zone to moderate the computational values and the

analytical values given by wave theory. The relaxation function proposed by Jacobsen *et al.* (2011) presented in Eq. (5) is used in this study.

$$\Gamma(x) = 1 - \frac{\exp(x^{3.5}) - 1}{\exp(1) - 1} \text{ for } x \in [0;1] \quad (5)$$

where x is the coordinate along the x -axis scaled to the length of the relaxation zone. In the wave generation zone, the values for the free surface elevation and the velocity given by wave theory are prescribed to the computational values using the relaxation function $\Gamma(x)$ as shown in Eq. (6) and the generated waves are released into the working zone of the wave tank. In the wave absorption zone, the relaxation function is operated as $\Gamma(1-x)$. The computational values of velocity and free surface from the working zone are reduced to zero and the wave energy is smoothly removed from the computational domain.

$$\begin{aligned} u_{relaxed} &= \Gamma(x)u_{analytical} + (1 - \Gamma(x))u_{computational} \\ \phi_{relaxed} &= \Gamma(x)\phi_{analytical} + (1 - \Gamma(x))\phi_{computational} \end{aligned} \quad (6)$$

Linear waves are produced in the numerical wave tank using the relaxation method by prescribing the values for the free surface η , the horizontal particle velocity u and the vertical particle velocity w as shown in Eq. (7), (8) and (9) respectively.

$$\eta = a \cos(\omega t - kx) \quad (7)$$

$$u = \omega a \frac{\cosh k(z+d)}{\sinh kd} \sin(\omega t - kx) \quad (8)$$

$$w = \omega a \frac{\sinh k(z+d)}{\sinh kd} \cos(\omega t - kx) \quad (9)$$

where a is the wave amplitude, ω is the angular wave frequency, d is the water depth, $k=2\pi/L$ is the wave number. Similarly, higher order waves are generated in the wave tank using the appropriate relations for the free surface and the water particle velocity.

3. Results and Discussion

A grid convergence study is carried out to verify good wave generation and propagation. A 2D numerical wave tank 38m long and 0.8m high is used to generate second-order Stokes waves of wave height $H=0.022$ m and wave period $T=2.525$ s in a water depth of $d=0.4$ m on grid sizes $dx=0.05$ m, 0.025 m, 0.01 m. It is seen from the results in Fig. 1 that the wave height converges to the desired waveform from a grid size of $dx=0.025$ m. In order to capture the wave transformation in the simulations with good accuracy, a finer grid size of $dx=0.01$ m is chosen for the simulations.

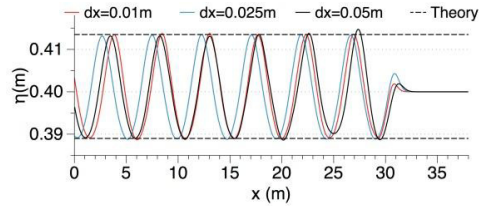


Fig. 1. Grid convergence study in the numerical wave tank with $T=2.525s$ and $H=0.022m$ in a water depth $d=0.4m$

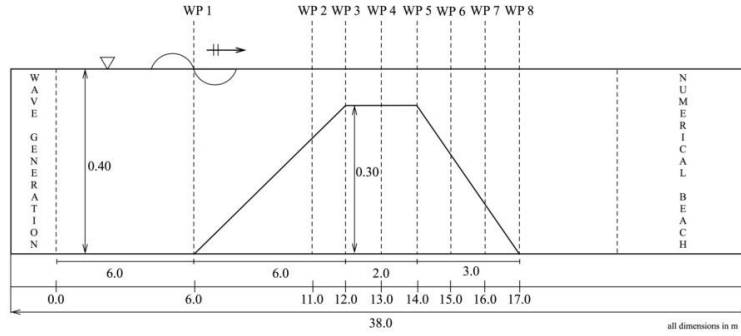


Fig. 2. Schematic diagram of the numerical wave tank setup used to simulate wave propagation over a submerged bar

Simulations are carried out in a 2D numerical wave tank 38m long and 0.8m high with a grid resolution of $dx=0.01m$ resulting in a total of 304000 cells. A submerged trapezoidal bar is placed at a distance of 6.0m from the wave generation zone with a crest height of 0.3m in a water depth $d=0.4m$. The bar has a seaward slope of 1:20 and a leeward slope of 1:10. The maximum water depth over the crest of the bar is 0.1m. Wave gages are placed in the numerical wave tank at 6.0m, 11.0m, 12.0m, 13.0m, 14.0m, 15.0m, 16.0m and 17.0m from the end of the wave generation zone as shown in Fig. 2.

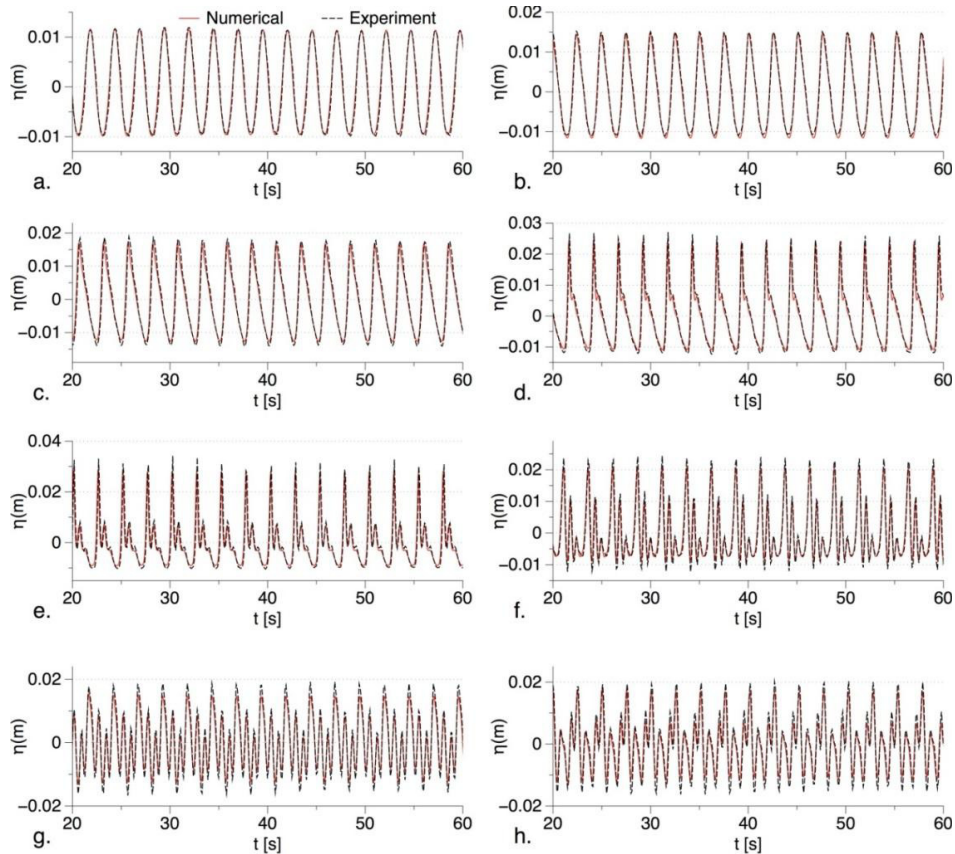


Fig. 3. Wave transformation for $H=0.022\text{m}$: (a) WP 1: 6m; (b) WP 2: 11m; (c) WP 3: 12m; (d) WP 4: 13m; (e) WP 5: 14m; (f) WP 6: 15m; (g) WP 7: 16m; (h) WP 8: 17m.

Second-order Stokes waves of period $T=2.525\text{s}$ and height $H=0.022\text{m}$ are generated. The transformation of the wave as it propagates over the bar is computed using the wave gages placed in the numerical wave tank and the results are compared with the experimental data in Fig. 3. The free surface measured at the base of the submerged bar (WP 1) in Fig. 3a is considered to be the incident wave on the submerged bar. The horizontal asymmetry in the wave profile of the incident waves is seen with the crest height being slightly higher than the trough depth. The wave is deformed due to shoaling on a reducing water depth as it propagates up the seaward slope. The increase in the free surface elevation at WP 2 is seen in Fig. 3b. The wave reaches the crest of the bar and propagates over the flat bottom with a water depth of $d=0.1\text{m}$ and Fig. 3c shows the vertical asymmetry in the waveform at WP 3. The decomposition of the wave begins at WP 4 in Fig. 3d resulting in the appearance of a secondary crest after the primary wave crest. In Fig. 3e, the waveform with the transformed incident wave and a clearly developed secondary crest is seen at WP 5, at the end of the bar crest. From this point onwards, the leeward slope of the bar begins and the water depth increases along the direction of wave propagation. The amplitudes of the waves begin to reduce in an effect opposite to shoaling, as the waves propagate from shallower water to deeper water. The development of a tertiary crest is seen in Fig. 3f along with the developed secondary crest at WP 6. As the wave propagates further along the leeward slope of the bar, the well developed secondary and tertiary crests are clearly seen in Figs. 3g and 3h at WP 7 and WP 8 respectively. A good agreement is seen between the numerical results and the experimental data and the numerical model provides a good representation of the phase and amplitude of the transformed wave.

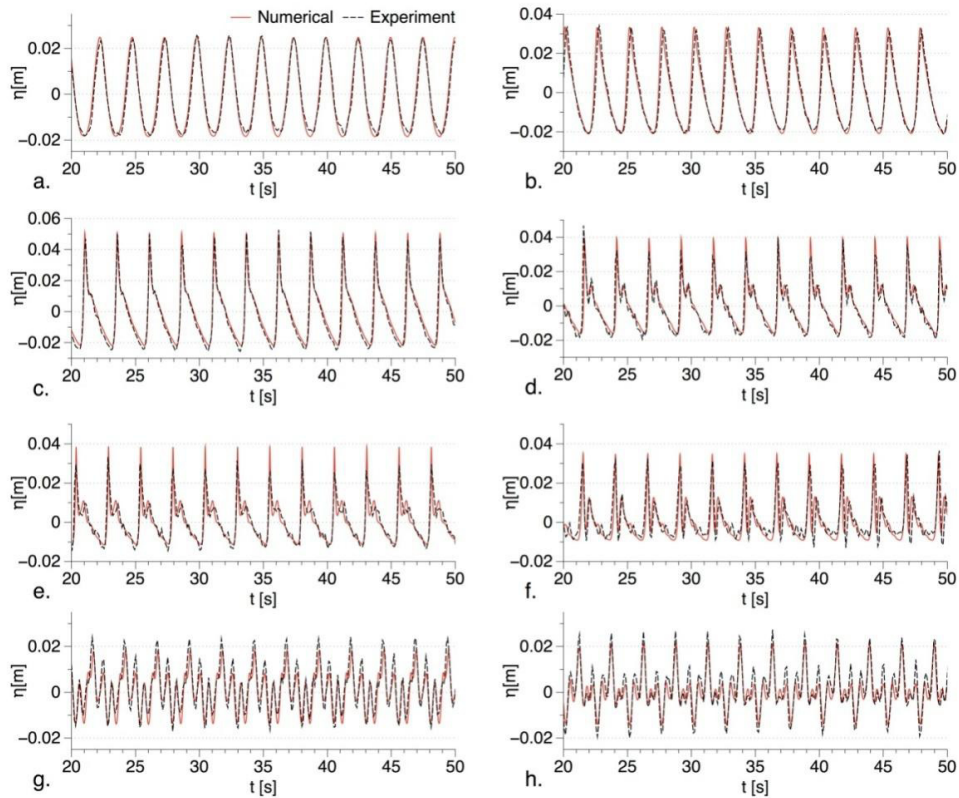


Fig. 4. Wave transformation for $H=0.044\text{m}$: (a) WP 1: 6m; (b) WP 2: 11m; (c) WP 3: 12m; (d) WP 4: 13m; (e) WP 5: 14m; (f) WP 6: 15m; (g) WP 7: 16m; (h) WP 8: 17m.

Further, a simulation is carried out with an incident wave height of $H=0.044\text{m}$, period $T=2.525\text{s}$. The effect of the increased incident wave height on the wave deformation over the submerged bar is investigated. The comparison of the numerical results with the experimental data is presented in Fig. 4. Due to the increased incident wave amplitude, the corresponding shoaling effect is also higher at WP 3 as the wave reaches the crest of the bar. The pattern of wave transformation in Fig. 3 for $H=0.022\text{m}$ and in Fig. 4 for $H=0.044\text{m}$ are similar but with a few differences in the transformed waveform. The saw tooth asymmetry in the wave form is seen to develop earlier at WP 2, as the wave propagates on the upward slope in this case. The formation of sharp crests is seen in Fig. WP 3 as the wave reaches the bar crest. A similar wave profile is seen in the previous case with a lower incident wave height, after the wave has reached the bar crest at WP 4 in Fig. 3. The formation of a distinct secondary crest is seen at WP 4 in Fig. 4d. The transfer of wave energy to the higher harmonics and formation of clear secondary and tertiary wave crests is slower in this case and the wave profiles at WP 4 and WP 5 are similar. The appearance of a distinct secondary crest and smaller tertiary crests is seen at WP 6, as the wave propagates on the leeward slope of the bar. It is noticed that the secondary peaks are much lower than the primary peaks in this case. Figure WP 7 shows the evolution of the transformed waveform with three distinct crests of different amplitudes. This transformation is already apparent at an earlier location at WP 6 in Fig. 3, in the case of the lower incident wave height. At the end of the leeward slope, in WP 8, the secondary and tertiary crests are seen to have similar amplitudes which are much lower than the primary crest. Although the shoaling of the higher amplitude waves is seen at an earlier location compared to the lower amplitude waves, the wave decomposition over the bar crest and the leeward slope is seen at later locations. This is because the higher amplitude waves propagate faster over the bar crest than the lower amplitude waves, resulting in lesser interaction time between the wave and the flat bottom. It is seen that the

numerical model is able to accurately represent the phase information of the deformed wave though slight deviations are seen wave crest heights due to the complex wave transformation processes involved.

The simulations with wave transformation over a submerged bar show that the amount of shoaling depends on the incident wave height. A wave with a higher incident amplitude shows more shoaling on the upward slope of the submerged bar. The incident wave profile transforms into an asymmetrical wave with form sharp wave crests and shallow troughs in both the cases. A higher asymmetry with sharp crests can lead to wave instability, resulting in wave breaking. As seen in Figs. 3 and 4, the numerical results show a good match to the experimental data and the model is able to provide a good representation of the wave propagation and transformation.

Conclusion

The open source CFD model REEF3D is used to simulate the wave propagation and transformation over a submerged bar. The numerical results are compared to the experimental data and a good agreement is seen. The wave transformation is clearly observed with the formation of an asymmetrical wave profile with sharper crests and shallower troughs as the wave propagates over the upward slope of the submerged bar. The evolution of higher harmonics during the wave propagation is seen for both cases of incident wave heights simulated. The appearance of the higher harmonics in the wave train is slightly delayed for higher incident waves and the higher harmonics are seen have similar crest heights that are lower than the primary wave crest. Thus, the wave transformation depends on the incident wave height. The higher incident waves show more shoaling as they propagate on the upward slope. Further studies can be carried out to investigate the transition of the waves into a wave breaking regime, on further increasing the incident wave height.

Acknowledgements

The authors are grateful to Prof. Serdar Beji, Istanbul Technical University for providing the experimental data. This study has been carried out under the OWCBW project (No. 217622/E20) and the authors are grateful to the grants provided by the Research Council of Norway. This study was supported in part by computational resources provided at NTNU by NOTUR <http://www.notur.no>.

References

- Alagan Chella, M., Bihs, H., Myrhaug, D. and Muskulus, M. (2015). Breaking characteristics and geometric properties of spilling breakers over slopes. *Coastal Engineering* 95: 4-19.
- Beji, S. and Battjes, J. A. (1993). Experimental investigation of wave propagation over a bar. *Coastal Engineering* 19: 151-162.
- Beji, S. and Battjes, J. A. (1994). Numerical simulation of nonlinear wave propagation over a bar. *Coastal Engineering* 23: 1-16.
- Berthelsen, P. A. and Faltinsen, O. M. (2008). A local directional ghost cell approach for incompressible viscous flow problems with irregular boundaries. *Journal of Computational Physics* 227: 4354-4397.
- Bihs, H. (2011). Three-dimensional numerical modeling of local scouring in open channel flow, Department of Hydraulic and Environmental Engineering, Norwegian University of Science and Technology, Trondheim, Norway.
- Blenkinsopp, C. E. and Chaplin, J. R. (2008). The effect of crest submergence on wave breaking over submerged slopes. *Coastal Engineering* 55: 967-974.
- Bradshaw, P., Ferriss, D. H. and Atwell, N. P. (1967). Calculation of boundary layer development using the turbulent energy equation. *Journal of Fluid Mechanics* 28: 593-616.
- Brocchini, M., Drago, M. and Iovenitti, L. (1992). The modelling of short waves in shallow waters. Comparison of numerical methods based on Boussinesq and Serre equations. *Proceedings of the 23rd International Conference on Coastal Engineering*, New York, ASCE.
- Chang, K.-A., Hsu, T.-J. and Liu, P. L.-F. (2001). Vortex generation and evolution in water waves propagating over a submerged rectangular obstacle Part I. Solitary waves. *Coastal Engineering* 44: 13-36.
- Chorin, A. (1968). Numerical solution of the Navier-Stokes equations. *Mathematics of Computation* 22: 745-762.
- Christensen, E. D. (1998). Turbulence in breaking waves- A numerical investigation. PhD Thesis, Technical

University of Denmark.

- Durbin, P. A. (2009). Limiters and wall treatments in applied turbulence modeling. *Fluid Dynamics Research* 41: 1-18.
- Jacobsen, N. G., Fuhrman, D. R. and Fredsøe, J. (2011). A wave generation toolbox for the open-source CFD library: OpenFOAM. *International Journal for Numerical Methods in Fluids* 70(9): 1073-1088.
- Jiang, G. S. and Shu, C. W. (1996). Efficient implementation of weighted ENO schemes. *Journal of Computational Physics* 126: 202-228.
- Kobayashi, N., Otta, A. and Roy, I. (1987). Wave reflection and run-up on rough slopes. *Journal of Waterway, Port, Coastal and Ocean Engineering* 113(3): 282-298.
- Mayer, S., Garapon, A. and Sørensen, L. S. (1998). A fractional step method for unsteady free surface flow with applications to non-linear wave dynamics. *International Journal for Numerical Methods in Fluids* 28: 293-315.
- Naot, D. and Rodi, W. (1982). Calculation of secondary currents in channel flow. *Journal of the Hydraulics Division, ASCE* 108(8): 948-968.
- Osher, S. and Sethian, J. A. (1988). Fronts propagating with curvature- dependent speed: algorithms based on Hamilton-Jacobi formulations. *Journal of Computational Physics* 79: 12-49.
- Peng, D., Merriman, B., Osher, S., Zhao, H. and Kang, M. (1999). A PDE-based fast local level set method. *Journal of Computational Physics* 155: 410-438.
- Shu, C. W. and Osher, S. (1988). Efficient implementation of essentially non-oscillatory shock capturing schemes. *Journal of Computational Physics* 77: 439-471.
- Ting, F. C. K. and Kirby, J. T. (1996). Dynamics of surf-zone turbulence in a spilling breaker. *Coastal Engineering* 27: 131-160.
- van der Vorst, H. (1992). BiCGStab: A fast and smoothly converging variant of Bi-CG for the solution of nonsymmetric linear systems. *SIAM Journal on Scientific and Statistical Computing* 13: 631-644.
- Wilcox, D. C. (1994). *Turbulence modeling for CFD*, DCW Industries Inc., La Canada, California.